Robust interferometry against imperfections based on weak value amplification

Chen Fang, Jing-Zheng Huang,* and Guihua Zeng†

State Key Laboratory of Advanced Optical Communication Systems and Networks, Center of Quantum Information Sensing and Processing, Shanghai Jiao Tong University, Shanghai 200240, China

(Received 15 March 2018; published 11 June 2018)

Optical interferometry has been widely used in various high-precision applications. Usually, the minimum precision of an interferometry is limited by various technical noises in practice. To suppress such kinds of noises, we propose a scheme which combines the weak measurement with the standard interferometry. The proposed scheme dramatically outperforms the standard interferometry in the signal-to-noise ratio and the robustness against noises caused by the optical elements' reflections and the offset fluctuation between two paths. A proof-of-principle experiment is demonstrated to validate the amplification theory.

DOI: 10.1103/PhysRevA.97.063818

I. INTRODUCTION

The optical interferometry has been widely used in science and industry fields such as physics [1], astronomy [2], engineering [3], applied science [4], biology [5], and medicine [6]. In all of these applications, an important issue is to detect the length difference or the phase difference between different paths. Making use of the obtained differences, one may achieve a high-precision length measurement [1]. Theoretically, the minimum measurable length difference is limited by the shot-noise limit [7], which is inversely proportional to the square root of the input intensity and the number of measurement events, while in practice the technical noises may cause uncertainty that is usually much higher than the theoretical limit. Hence, suppression of the practical technical noises has become an important issue in applications of interferometry.

Aiming at high-precision detection, a technique called weak value amplification (WVA) [8–15] can suppress the technical noises to increase the signal-to-noise ratio (SNR). This has been demonstrated in theories [16–18] and experiments [12,13]. Physically, such suppression can be achieved by amplifying the signal at the cost of decreasing the probability of detection. Due to the amplification, small changes beyond the detector resolution can even be detected [9,10].

In this paper, we propose a scheme named weak-value-amplified interferometry (WVAI) which merges the WVA and the standard interferometry (SI) together. By applying the WVA technique, this scheme amplifies the phase difference before detection in an interferometer. The amplification provides the robustness against technical noises. Based on an optical Mach-Zehnder interferometer, the performance of the proposed scheme is investigated. Then the influences of two kinds of technical noises, which are respectively caused by the reflections of the optical elements and the fluctuations of the phase offset, are studied. The results show that the WVAI scheme outperforms the SI in the SNR and in the technical noise suppression. In addition, a proof-of-principle experiment is demonstrated to verify the phase amplification effect of the WVAI scheme.

This paper is organized as follows. In Sec. II we present an interferometry scheme referred to as WVAI. Then the influences of two typical technical noises, which are respectively caused by the reflections of the optical elements and the fluctuations of the offset between two paths, are investigated in Sec. III. In Sec. IV a proof-of-principle experiment is demonstrated and analyzed. Section V summarizes the paper.

II. SCHEME DESCRIPTION

Before presenting the proposed scheme, let us consider an optical Mach-Zehnder interferometer to exemplify the standard interferometry. Displayed in Fig. 1(a), a monochromatic laser beam is split into two paths by the beam splitter BS1 with a 50:50 splitting ratio. In the lower path, $e^{-i\theta}$ stands for the phase difference between the two paths. In the upper path, a controllable phase ϕ is introduced as an offset phase delay. The two beams in the two paths interfere after recombining by BS2. Then one can collect the output intensity of the interference by a detector, which is

$$I_{\phi I}(\theta) = I_{\text{in}}\left|\frac{e^{-i\phi}+e^{-i\theta}}{2}\right|^2 = \frac{I_{\text{in}}}{2}[1+\cos(\phi-\theta)], \quad (1)$$

where I_{in} is the input light intensity. The subscripts I and ϕ represent the SI scheme and the phase offset, respectively.

With a little modification, one can combine the interferometer with the WVA technique. As indicated in Fig. 1(b), two linear polarizers are inserted before BS1 and after BS2, respectively. These polarizers are used to select the system in the preselected state $|\psi_i\rangle = 1/\sqrt{2}(|H\rangle + |V\rangle)$ and in the postselected state $|\psi_f\rangle = \cos\alpha|H\rangle + \sin\alpha|V\rangle)$, respectively. Note that H and V stand for the horizontal and vertical polarized directions, respectively. The phase difference $e^{-i\theta}$ is replaced with a unitary operation $\hat{U}(\theta) = e^{-i\theta\hat{A}}$, where $A \equiv |H\rangle\langle H| - |V\rangle\langle V|$. Then one obtains a WVAI scheme based on an optical Mach-Zehnder interferometer. Other types

*jzhuang1983@sjtu.edu.cn
†ghzeng@sjtu.edu.cn

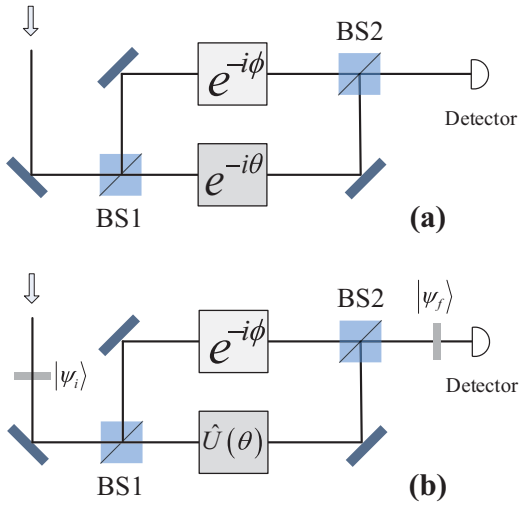

FIG. 1. Schematic diagram of (a) SI and (b) WVAI based on an optical Mach-Zehnder interferometer.

of interferometers, such as Michelson, Sagnac, and atom interferometers, will be straightforward.

The output state of the modified interferometer is expressed as

$$|\Psi_{\text{out}}\rangle = \langle\psi_f|\frac{e^{-i\phi}+\hat{U}(\theta)}{2}|\psi_i\rangle|\phi(p)\rangle, \tag{2}$$

where $|\phi(p)\rangle$ is the input laser state and p stands for the momentum. When $\alpha = -\pi/4+\epsilon$ and $|\theta/\epsilon| \ll 1$, the output state could be written in its first-order approximation

$$|\Psi_{\text{out}}\rangle \approx \langle\psi_f|\psi_i\rangle\frac{e^{-i\phi}+e^{-iA_w\theta}}{2}|\phi(p)\rangle, \tag{3}$$

where

$$A_w = \frac{\langle\psi_f|\hat{A}|\psi_i\rangle}{\langle\psi_f|\psi_i\rangle} = \frac{\cos\alpha-\sin\alpha}{\cos\alpha+\sin\alpha} = \cot\epsilon. \tag{4}$$

The detector collects the light selected by $|\psi_f\rangle$. The detected intensity is given by

$$I_{\phi A}(\theta) \approx I_{\text{in}}|\langle\psi_f|\psi_i\rangle|^2\left|\frac{e^{-i\phi}+e^{-iA_w\theta}}{2}\right|^2$$
$$= \frac{I_{\text{in}}\sin^2\epsilon}{2}[1+\cos(\phi-A_w\theta)], \tag{5}$$

where the subscript A indicates the proposed scheme. Because of the postselection, the orthogonal polarized parts are neglected. The successful selected probability is $\sin^2\epsilon$. For the purpose of amplifying the phase difference, ϵ should be far less than 1. Note that $|\theta/\epsilon| \ll 1$ still needs to be satisfied. Under both approximate conditions, Eq. (5) becomes

$$I_{\phi A}(\theta) \approx \frac{I_{\text{in}}}{2A_w^2}[1+\cos(\phi-A_w\theta)]. \tag{6}$$

Figure 2 shows the output intensity of different offsets without phase delay input ($\theta = 0$) in SI. Based on the WVAI scheme, one may get a similar curve with an attenuation of $1/A_w^2$ in the amplitude. Typically, the offset ϕ is set at two phase values, i.e., $\pi/2$ and π, for the highest sensitivity and the weak signal detection, respectively.

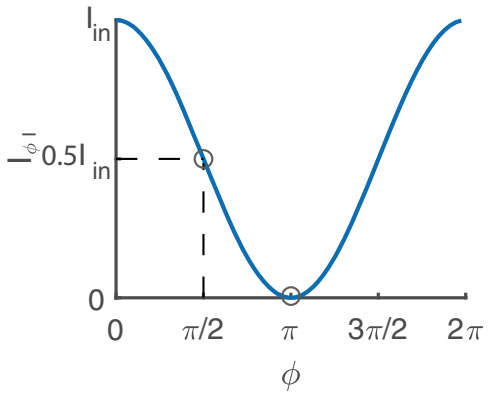

FIG. 2. Output intensity $I_{\phi I}$ of different offsets ϕ without phase delay input ($\theta = 0$) in standard interferometry.

In applications, it is more common to detect the output intensity difference between no phase delay input and θ ($\theta > 0$) input, which is

$$\Delta I_\phi(\theta) = I_\phi(\theta) - I_\phi(0).$$

This difference can be obtained by differential detection [19] or phase and amplitude modulation [20]. Without the technical noises, the detection uncertainty is inversely proportional to the square root of ΔI_ϕ. We will compare the intensity difference of WVAI with that of SI in the following.

When $\phi = \pi$, the interferometer has total destructive interference. Since it is easier to detect a brightening of nothing than to detect a dimming of a bright light, this offset is usually set for weak signal detection like gravitational wave detection. Omitting the technical noise, ΔI_ϕ is equal to the detected intensity in both the WVAI and the SI scheme, which can be written in the first-order approximation as, respectively,

$$\Delta I_{\pi A} = I_{\pi_A} \approx I_{\text{in}}\theta^2/4, \quad \Delta I_{\pi I} = I_{\pi_I} \approx I_{\text{in}}\theta^2/4, \tag{7}$$

where the subscript π means the phase offset is set at π. Explicitly, the output intensity difference is proportional to the quadratic term of θ. The two schemes hold the same uncertainty. Although θ has been amplified, the WVAI scheme detects the same intensity as the SI. This degradation is responsible for discarding light in the postselection.

When $\phi = \pi/2$, this offset leads to a maximum sensitivity of the interferometer. In Fig. 2, it can be seen that the curve has a maximum gradient with $\phi = \pi/2$. In this situation,

$$\Delta I_{(\pi/2)A} \approx \frac{0.5I_{\text{in}}\sin(A_w\theta)}{A_w^2} \approx \frac{0.5I_{\text{in}}\theta}{A_w},$$
$$\Delta I_{(\pi/2)I} \approx 0.5I_{\text{in}}\sin\theta \approx 0.5I_{\text{in}}\theta. \tag{8}$$

Obviously, $\Delta I_{(\pi/2)A}$ is smaller than $\Delta I_{(\pi/2)I}$ by a factor of $1/A_w$ because of the low probability of postselection. It seems like the WVAI scheme has no advantage over the SI schemes in this situation. However, when technical noises are taken into consideration, the WVAI appears to become more robust compared with the SI.

In order to explain the noise resistance, we introduce the intensity contrast ratio (ICR), which is expressed as

$$C_\phi = I_\phi(\theta)/I_\phi(0).$$

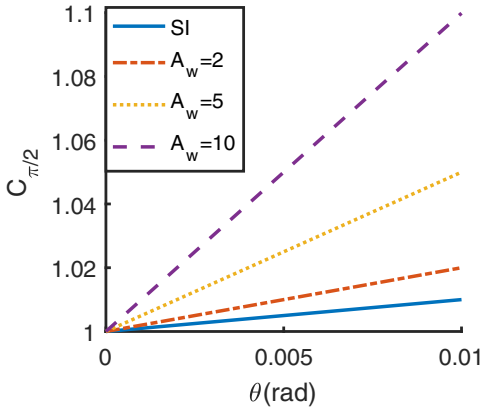

FIG. 3. Intensity contrast ratio with the offset $\phi = \pi/2$ of SI (solid line), $A_w = 2$ (dash-dotted line), $A_w = 5$ (dotted line), and $A_w = 10$ (dashed line).

The ICR represents the ratio of the intensity variation (detected signal) induced by the phase delay to the postselected light intensity [21]. The ICRs of the SI and the WVAI can be written, respectively, as

$$C_{\phi I} = \frac{1+\cos(\phi-\theta)}{1+\cos\phi}, \quad C_{\phi A} = \frac{1+\cos(\phi - A_w\theta)}{1+\cos\phi}. \tag{9}$$

We are interested in the case of $\phi = \pi/2$. In this case, $C_{(\pi/2)A}$, which increases along with the increase of A_w, is larger than $C_{(\pi/2)I}$ when $A_w > 1$, as depicted in Fig. 3.

A larger intensity contrast ratio implies that a greater proportion of the detected intensity is occupied by the signal. If the noise is relative to the detected intensity, e.g., the relative intensity noise (RIN) [22], which is the main factor causing detection uncertainties in some applications [23], the greater proportion will result in a higher SNR. The relationship between the RIN and the detected intensity is $\sigma^{(n)}_{\mathrm{RIN}} = \beta I(\theta)$, where β is the coefficient. When measuring the intensity difference, the SNR can be expressed as

$$\frac{\Delta I}{\sigma^{(n)}_{\mathrm{RIN}}} = \frac{\Delta I}{I(\theta)}\frac{I(\theta)}{\sigma^{(n)}_{\mathrm{RIN}}} = \left(1-\frac{1}{C}\right)\frac{1}{\beta}. \tag{10}$$

Apparently, the larger C indicates stronger robustness against the RIN. When $0 \leqslant \phi \leqslant \pi$ and $0 < A_w\theta \ll 1$, it is easy to verify that $C_{\phi A} < C_{\phi I}$. Thus the WVAI scheme has a higher SNR under the same RIN than that of the SI. In practice, the relationship between the technical noises and the detected intensity may be more complicated. However, the higher intensity contrast ratio can still provide a better noise resistance. A detailed analysis will be shown in the next section.

Finally, if the power-recycle technique [24] is taken into consideration, all the light will go through the postselection without attenuation. One may gain a magnificence A_w^2 times that of the output intensity, which is

$$I_{\phi A}(\theta) \approx \frac{I_{\mathrm{in}}}{2}[1+\cos(\phi - A_w\theta)]. \tag{11}$$

The amplified phase will boost the performance with any ϕ. With balanced differential detectors, a $\pi/2$ offset will lead to an enhancement of sensitivity A_w times that of SI.

III. IMPERFECTION ANALYSIS

In this section, we discuss two typical kinds of technical noises as examples to demonstrate the robustness of the proposed scheme against the noises. These noises are caused by the reflections of imperfect optical elements and the fluctuation of the offset ϕ, respectively.

A. Reflection of imperfect optical elements

In practice, the ratio of all the optical elements' transmission cannot be 1. The reflected light will interfere with the output light field. For example, in the proposed scheme depicted in Fig. 1, the imperfections of BS1, BS2, and all the mirrors could cause this problem. The reflected light field before postselection can be written as $E_{\mathrm{in}}\eta_n e^{i\delta_n}$, where the subscript n denotes the number of the optical elements and E_{in}, η_n, and δ_n are the input light field, the square root of the reflectivity, and the relative phase of corresponding elements, respectively. Generally, one has the expression

$$\eta e^{i\delta} = \sum_{n=1}^{N} \eta_n e^{i\delta_n},$$

where N is the total number of optical elements, $\eta = \sqrt{\sum_{n=1}^{N}\eta_n^2}$, and $\tan\delta = \frac{\sum_{n=1}^{N}\sin\delta_n}{\sum_{n=1}^{N}\cos\delta_n}$. Commonly, $\eta \ll 1$ and δ can be any value from $-\pi$ to π. Then the output intensity described by Eq. (6) becomes

$$\begin{aligned} I_{1A}(\theta) &\approx I_{\mathrm{in}}|\langle\psi_f|\psi_i\rangle|^2\left|\frac{e^{-i\phi}+e^{-iAw\theta}+\sum_{n=1}^{N}\eta_n e^{i\delta_n}}{2}\right|^2 \\ &\approx \frac{I_{\mathrm{in}}}{2A_w^2}\left\{1+\frac{\eta^2}{2}+\cos(\phi-A_w\theta)\right. \\ &\quad \left.+\eta[\cos(\phi+\delta)+\cos(A_w\theta+\delta)]\right\}. \end{aligned} \tag{12}$$

When $\phi = \pi$, according to the Taylor expansion to the second order in Eq. (12), one acquires

$$\Delta I_{1A}(\theta) \approx \left(S_{1A} + \sigma^{(n)}_{1A}\right) I_{\mathrm{in}},$$

where

$$S_{1A} = \frac{\theta^2}{4}, \quad \sigma^{(n)}_{1A} = \frac{\eta^2}{4A_w^2} - \eta\left(\frac{\theta^2}{2}\cos\delta + \frac{\theta\sin\delta}{A_w}\right). \tag{13}$$

Here S_{1A} and $\sigma^{(n)}_{1A}$ are the proportions of the input intensity, that is, the signal induced by phase delay θ and the noise caused by the reflected light, respectively. In contrast, in SI, one has

$$\Delta I_{1I}(\theta) \approx \left(S_{1I} + \sigma^{(n)}_{1I}\right) I_{\mathrm{in}},$$

where

$$S_{1I} = \frac{\theta^2}{4}, \quad \sigma^{(n)}_{1I} = \frac{\eta^2}{4} - \eta\left(\frac{\theta^2}{2}\cos\delta + \theta\sin\delta\right). \tag{14}$$

To reveal the noise influences in both schemes, we compare the absolute value of $\sigma^{(n)}$ in Eqs. (13) and (14) with $\eta = 0.01$. The results are shown in Fig. 4. When $A_w \geqslant 10$ the noise of the WVAI is at least one order of magnitude lower than that of the SI, leading to a higher SNR. The SNR with $\eta = 0.01$ and $\delta = 0$ can been seen in Fig. 5. In addition, compared

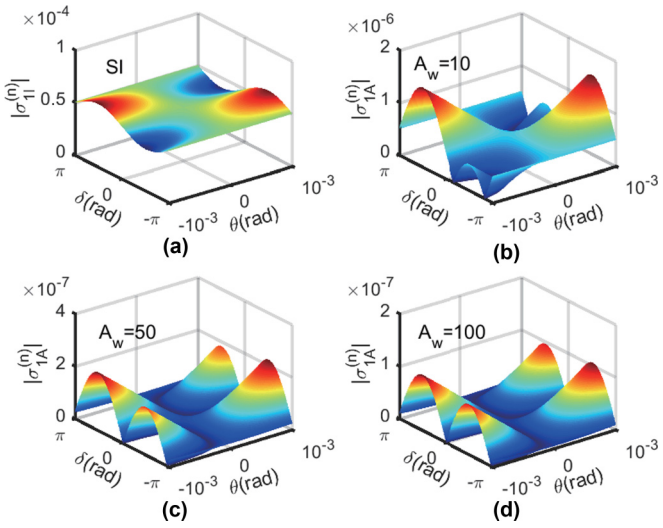

FIG. 4. Calculated results of $|\sigma_1^{(n)}|$ in Eqs. (13) and (14) with $\eta = 0.01$ and an offset $\phi = \pi$.

among Figs. 4(b)–4(d) and 5, as long as the amplification factor increases, the noise decreases, leading to an increasing SNR.

When $\phi = \pi/2$, the intensity difference in the WVAI scheme is given by

$$\Delta I_{2A}(\theta) \approx \left(S_{2A} + \sigma_{2A}^{(n)}\right) I_{\text{in}},$$

where

$$S_{2A} = \frac{\theta}{2A_w}, \quad \sigma_{2A}^{(n)} = \eta\left(\frac{1-\eta}{A_w^2} - \frac{\theta^2}{4}\cos\delta - \frac{\theta\sin\delta}{2A_w}\right). \tag{15}$$

In contrast, in the SI scheme, the intensity difference is given by

$$\Delta I_{2I}(\theta) \approx I_{\text{in}}\left(S_{2I} + \sigma_{2I}^{(n)}\right),$$

where

$$S_{2I} = \tfrac{\theta}{2}, \quad \sigma_{2I}^{(n)} = \eta\left(1 - \eta - \tfrac{\theta^2}{4}\cos\delta - \tfrac{\theta\sin\delta}{2}\right). \tag{16}$$

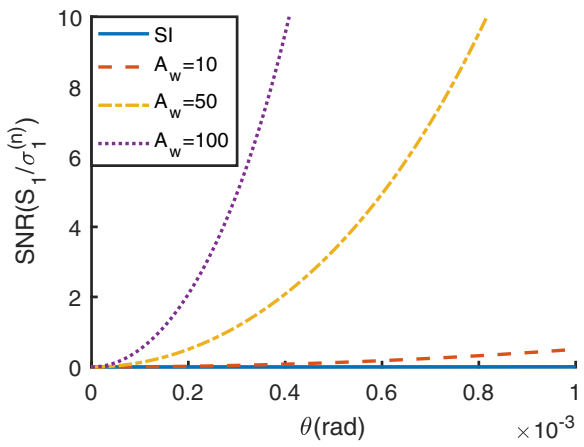

FIG. 5. The SNRs of SI (solid line), $A_w = 10$ (dashed line), $A_w = 50$ (dash-dotted line), and $A_w = 100$ (dotted line), calculated with $\eta = 0.01$, $\delta = 0$, and an offset $\phi = \pi$.

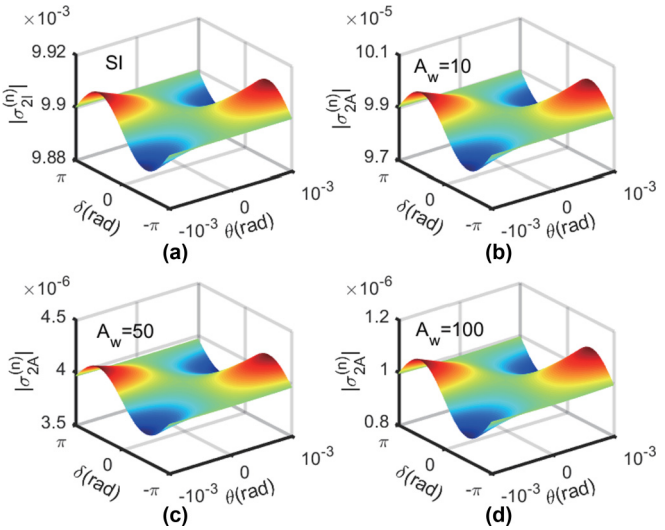

FIG. 6. Calculated results of $|\sigma_2^{(n)}|$ in Eqs. (15) and (16) with $\eta = 0.01$ and an offset $\phi = \pi/2$.

Similarly, the results of $|\sigma^{(n)}|$ with $\eta = 0.01$ are depicted in Fig. 6. The noise in the WVAI scheme is at least two orders of magnitude less than that of the SI. From Fig. 7, although the collected intensity in the WVAI is $1/A_w$ of that of the SI with the same θ, the SNR of the WVAI is still higher than that of the SI.

B. Fluctuations of offset ϕ

Vibrations, air movements, deformations of optical mounts, and other environmental factors may change the path difference between two arms of the interferometer. These effects cause fluctuations of ϕ, which results in unexpected noises. Usually we use a closed-loop compensation to avoid the fluctuations. However, the fluctuations cannot be eliminated completely. Consider that there is a small fluctuation $\Delta\phi \ll 1$. Here $\Delta\phi$ must be less than θ; otherwise the signal will be submerged in

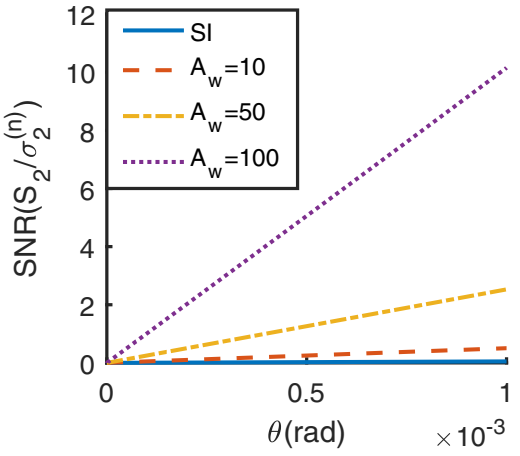

FIG. 7. The SNRs of SI (solid line), $A_w = 10$ (dashed line), $A_w = 50$ (dash-dotted line), and $A_w = 100$ (dotted line), calculated with $\eta = 0.01$, $\delta = 0$, and an offset $\phi = \pi/2$.

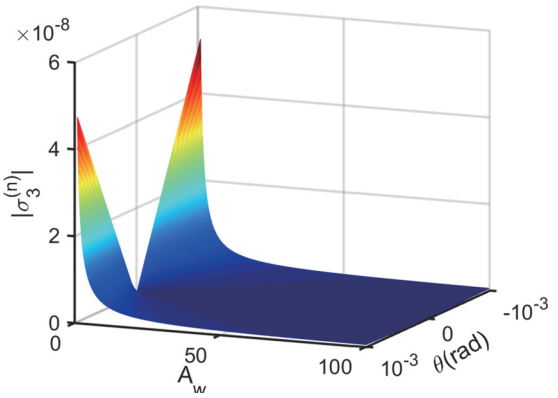

FIG. 8. Noise caused by the fluctuation of $\Delta\phi = 10^{-4}$ at the offset π calculated by Eq. (19).

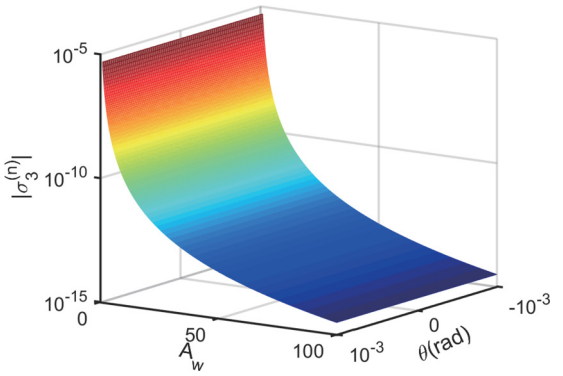

FIG. 9. Noise caused by the fluctuation of $\Delta\phi = 10^{-4}$ at the offset $\pi/2$ calculated by Eq. (20).

the noise. The output intensity difference is

$$\Delta I_{3A}(\theta) = I_{\text{in}}\left(S_{3A} + \sigma_{3A}^{(n)}\right),$$

where

$$S_{3A} = -\frac{I_{\text{in}}}{A_w^2}\sin\left(\phi - \frac{A_w\theta}{2}\right)\sin\left(\frac{A_w\theta}{2}\right),$$
$$\sigma_{3A}^{(n)} = \frac{1}{A_w^2}\sin\left(\phi - A_w\theta + \frac{\Delta\phi}{2}\right)\sin\frac{\Delta\phi}{2}. \quad (17)$$

For the SI, one obtains

$$\Delta I_{3I}(\theta) = I_{\text{in}}\left(S_{3I} + \sigma_{3I}^{(n)}\right),$$

where

$$S_{3I} = -I_{\text{in}}\sin\left(\phi - \frac{\theta}{2}\right)\sin\left(\frac{\theta}{2}\right),$$
$$\sigma_{3I}^{(n)} = \sin\left(\phi - \theta + \frac{\Delta\phi}{2}\right)\sin\frac{\Delta\phi}{2}. \quad (18)$$

Obviously, when $A_w = 1$, Eq. (17) is equal to Eq. (18). If one lets $\phi = \pi$, $|\sigma_3^{(n)}|$ becomes

$$|\sigma_3^{(n)}| = \left|\frac{1}{A_w^2}\sin\left(A_w\theta - \frac{\Delta\phi}{2}\right)\sin\frac{\Delta\phi}{2}\right|$$
$$\approx \left|\frac{(2A_w\theta - \Delta\phi)\Delta\phi}{4A_w^2}\right|. \quad (19)$$

When $|\theta| \leqslant |\Delta\phi|$, $|\sigma_3^{(n)}|$ decreases monotonically along $A_w \geqslant 1$, so the noise of the WVAI scheme is less than that of the SI scheme. The SNR of the WVAI scheme could benefit from the attenuated noise. The simulated results with $\Delta\phi = 10^{-4}$ rad are illustrated in Fig. 8. If one lets $\phi = \pi/2$, Eq. (19) becomes

$$|\sigma_3^{(n)}| = \left|\frac{1}{A_w^2}\cos\left(A_w\theta - \frac{\Delta\phi}{2}\right)\sin\frac{\Delta\phi}{2}\right|$$
$$\approx \left|\frac{\left(1 - A_w^2\theta^2 - \frac{\Delta^2\phi}{4} + A_w\theta\right)\Delta\phi}{4A_w^2}\right|, \quad (20)$$

where $|\sigma_3^{(n)}|$ also is monotonically decreases along $A_w \geqslant 1$ when $\phi = \pi/2$. Figure 9 is the calculated diagram with $\Delta\phi = 10^{-4}$ rad. Apparently, the SNR of the WVAI outperforms that of the SI with a $\pi/2$ offset.

IV. EXPERIMENT

As mentioned in Sec. II, the results of other types of interferometer are similar to the Mach-Zehnder type. Because it is easier to build and adjust, we choose instead a Michelson interferometer to demonstrate the proposed scheme. The experiment is set as illustrated in Fig. 10. A monochromatic laser beam, generated by a diode laser (Toptica, DL100) with a central wavelength of $\lambda_0 = 780$ nm, is prepared in the state $|\psi_i\rangle = 1/\sqrt{2}(|H\rangle + |V\rangle)$ by the first polarizer (labeled "Pre.") Then the beam enters a Michelson interferometer. The phase difference between two arms is $\phi + 2n\pi$, where n is an integer. The difference is set by the motor fixed on the mirror M2. After the beams recombine through the BS, a polarizer (labeled "Post") selects them at state $|\psi_f\rangle = \cos\alpha|H\rangle + \sin\alpha|V\rangle$. In both arms of the interferometer, we place a pair of waveplates to introduce a phase delay between horizontal and vertical polarization. It has been proved in [12,13] that the two waveplates could equivalently realize a thin birefringent

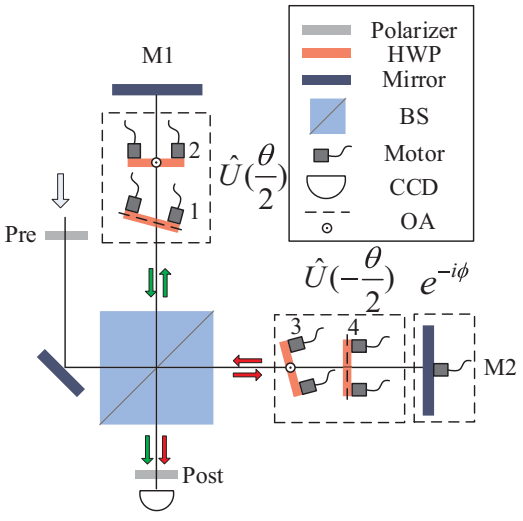

FIG. 10. Experimental setup: HWP, half-wave plate; BS, 50:50 beam splitter; and OA, optical axis.

crystal. The optical axes (OAs) of the half-wave plates (HWPs) are perpendicular to each other to cancel their phase delay. Tilting one of the HWPs around its OA by a tiny angle γ increases the optical path of this HWP, which introduces a unitary operation $\hat{U}(\theta) = e^{-i\theta A}$. In this experiment, the HWPs are binary compound zeroth-order half-wave plates, so the relationship between γ and θ is [13]

$$\theta = \frac{2\pi(n_e - n_o)h\gamma^2}{\lambda n^2}, \tag{21}$$

where n_e, n_o, and n are refractive indices of quartz for extraordinary light, ordinary light, and average light, respectively, h is the thickness of the plate, and λ is the wavelength of the light. The tilt also increases the optical path in one arm, which causes a variation of offset ϕ, so we put the HWPs into both arms to diminish this influence. As shown in Fig. 10, the OAs of HWP1 and HWP4 are in the horizontal direction and those of HWP2 and HWP3 are in the vertical direction. We tilt HWP1 and HWP3 along their OAs by the same angle γ to introduce opposite phase delay and to compensate for the increased optical path length.

By rotating the postselection polarizer to a different position, we could set the required A_w. The offset is set at π for the total destructive interference. However, the minimum step size of the motor on mirror M2 limits the practical accuracy of setting ϕ. The vibration of the optical platform and the deformation of the motor cause fluctuations of the offset. To prove the amplification effect, we use the intensity contrast ratio $C = I(\theta)/I(0)$ as a criterion. When $\phi > A_w\theta$, we obtain that

$$C_{\phi A} = \frac{I_\phi(\theta)}{I_\phi(0)} = \frac{1 + \cos(\phi - A_w\theta)}{1 + \cos\phi}. \tag{22}$$

When $|\psi_f\rangle = |H\rangle$, the experiment becomes a traditional Michelson interferometer with the path difference of $\phi - \theta$ between the two arms. In this situation the intensity contrast ratio becomes

$$C_{\phi I} = \frac{I_\phi(\theta)}{I_\phi(0)} = \frac{1 + \cos(\phi - \theta)}{1 + \cos\phi}, \tag{23}$$

which is the same as the standard interferometry result discussed before.

The experimental results are shown in Fig. 11. All curves fit well with Eqs. (22) and (23). We calculate that $\phi = 3.0711$, which meets the set value π mentioned before. Apparently, the intensity contrast ratio increases along the amplification factor A_w, as predicted in Sec. II. The results firmly support the amplification effect in the WVAI scheme.

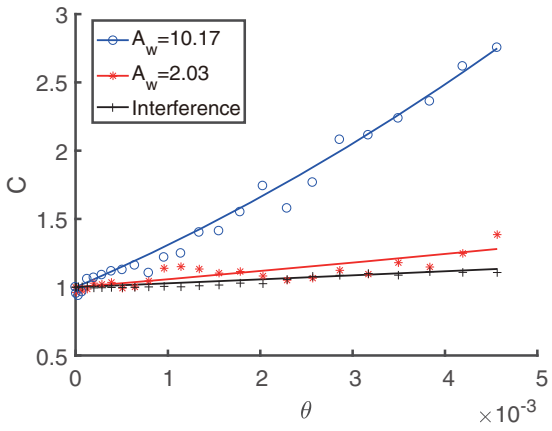

FIG. 11. Relation of the phase delay θ and intensity contrast ratio $I(\theta)/I(0)$. Blue circles, red plus signs and black asterisks are experimental results with $A_w = 10.17, 2.03$ and interference, respectively. $\phi = 3.0711$. The corresponding lines are fitting with Eq. (22) and Eq. (23).

V. CONCLUSION

We have proposed a scheme, named weak-value-amplified interferometry, which combines the weak value amplification and the standard interferometry. This scheme can amplify the phase difference between different paths at the cost of decreasing the detected probability. Although the proposed scheme has lower detected intensity than the standard interferometry, the investigation showed that it has a higher intensity contrast ratio and stronger robustness against technical noises. We demonstrated a proof-of-principle experiment based on a Michelson interferometer. The results successfully validate the phase amplification effect. Due to the ability of noise resistance, the proposed scheme may be applied on high-precision measurements such as gravitational wave detection, optical coherence tomography, and other phase detections. We believe that this scheme is a good alternative to the standard interferometry, where high sensitivity and strong noise resistance are required.

ACKNOWLEDGMENT

This work is supported by National Natural Science Foundation of China (Grant No. 61701302).

[1] B. P. Abbott *et al.* (LIGO Scientific and Virgo Collaborations), Tests of General Relativity with GW150914, Phys. Rev. Lett. **116**, 221101 (2016).

[2] J. D. Monnier, Optical interferometry in astronomy, Rep. Prog. Phys. **66**, 789 (2003).

[3] J. F. Biegen, Interferometric surface profiler, U.S. Patent No. 4,732,483 (22 March 1988).

[4] A. Lenef, T. D. Hammond, E. T. Smith, M. S. Chapman, R. A. Rubenstein, and D. E. Pritchard, Rotation Sensing with an Atom Interferometer, Phys. Rev. Lett. **78**, 760 (1997).

[5] R. D. Allen, N. Strömgren Allen, and J. L. Travis, Video-enhanced contrast, differential interference contrast (AVEC-DIC) microscopy: A new method capable of analyzing microtubule-related motility in the reticulopodial network of allogromia laticollaris, Cytoskeleton **1**, 291 (1981).

[6] D. Huang, E. A. Swanson, C. P. Lin, J. S. Schuman, W. G. Stinson, W. Chang, M. R. Hee, T. Flotte, K. Gregory, C. A. Puliafito, and J. G. Fujimoto, Optical coherence tomography, Science **254**, 1178 (1991).

[7] V. Giovannetti, S. Lloyd, and L. Maccone, Advances in quantum metrology, Nat. Photon. **5**, 222 (2011).
[8] Y. Aharonov, D. Z. Albert, and L. Vaidman, How the Result of a Measurement of a Component of the Spin of a Spin-1/2 Particle Can Turn out to be 100, Phys. Rev. Lett. **60**, 1351 (1988).
[9] O. Hosten and P. Kwiat, Observation of the spin Hall effect of light via weak measurements, Science **319**, 787 (2008).
[10] P. Ben Dixon, D. J. Starling, A. N. Jordan, and J. C. Howell, Ultrasensitive Beam Deflection Measurement via Interferometric Weak Value Amplification, Phys. Rev. Lett. **102**, 173601 (2009).
[11] G. I. Viza, J. Martínez-Rincón, G. A. Howland, H. Frostig, I. Shomroni, B. Dayan, and J. C. Howell, Weak-values technique for velocity measurements, Opt. Lett. **38**, 2949 (2013).
[12] X.-Y. Xu, Y. Kedem, K. Sun, L. Vaidman, C.-F. Li, and G.-C. Guo, Phase Estimation with Weak Measurement Using a White Light Source, Phys. Rev. Lett. **111**, 033604 (2013).
[13] C. Fang, J.-Z. Huang, Y. Yu, Q. Li, and G. Zeng, Ultra-small time-delay estimation via a weak measurement technique with post-selection, J. Phys. B **49**, 175501 (2016).
[14] O. S. Magaña-Loaiza, M. Mirhosseini, B. Rodenburg, and R. W. Boyd, Amplification of Angular Rotations Using Weak Measurements, Phys. Rev. Lett. **112**, 200401 (2014).
[15] M.-J. Hu and Y.-S. Zhang, Gravitational wave detection via weak measurements, arXiv:1707.00886.
[16] A. N. Jordan, J. Martínez-Rincón, and J. C. Howell, Technical Advantages for Weak-Value Amplification: when Less is More, Phys. Rev. X **4**, 011031 (2014).
[17] N. Brunner and C. Simon, Measuring Small Longitudinal Phase Shifts: Weak Measurements or Standard Interferometry? Phys. Rev. Lett. **105**, 010405 (2010).
[18] C.-F. Li, X.-Y. Xu, J.-S. Tang, J.-S. Xu, and G.-C. Guo, Ultrasensitive phase estimation with white light, Phys. Rev. A **83**, 044102 (2011).
[19] W. Denk, W. W. Webb, and A. J. Hudspeth, Mechanical properties of sensory hair bundles are reflected in their Brownian motion measured with a laser differential interferometer, Proc. Natl. Acad. Sci. U.S.A. **86**, 5371 (1989).
[20] B. Y. Kim and H. J. Shaw, Phase-reading, all-fiber-optic gyroscope, Opt. Lett. **9**, 378 (1984).
[21] X. Qiu, L. Xie, X. Liu, L. Luo, Z. Li, Z. Zhang, and J. Du, Precision phase estimation based on weak-value amplification, Appl. Phys. Lett. **110**, 071105 (2017).
[22] P. R. Morkel, R. I. Laming, and D. N. Payne, Noise characteristics of high-power doped-fibre superluminescent sources, Electron. Lett. **26**, 96 (1990).
[23] J. Blake and I. S. Kim, Distribution of relative intensity noise in the signal and quadrature channels of a fiber-optic gyroscope, Opt. Lett. **19**, 1648 (1994).
[24] Y.-T. Wang, J.-S. Tang, G. Hu, J. Wang, S. Yu, Z.-Q. Zhou, Z.-D. Cheng, J.-S. Xu, S.-Z. Fang, Q.-L. Wu, C.-F. Li, and G.-C. Guo, Experimental Demonstration of Higher Precision Weak-Value-Based Metrology Using Power Recycling, Phys. Rev. Lett. **117**, 230801 (2016).